

Perovskite Nanoparticles and Nanowires: Microwave–Hydrothermal Synthesis and Structural Characterization by High-Resolution Transmission Electron Microscopy

Xinhua Zhu,[†] Junyi Wang, Zhenghai Zhang, Jianmin Zhu, Shunhua Zhou, Zhiguo Liu, and Naiben Ming

National Laboratory of Solid State Microstructures, Department of Physics, Nanjing University, Nanjing 210093, China

Perovskite pure BaTiO₃ (BT) nanoparticles with spherical morphology and PX-phase PbTiO₃ (PT) nanowires with acicular morphology, were synthesized by microwave–hydrothermal process, and their atomic-scale microstructures were characterized by electron microscopy. Both X-ray diffraction (XRD) and selected area electron diffraction (SAED) patterns demonstrated that the produced BT nanoparticles remained a cubic perovskite structure at room temperature. The BT nanoparticles exhibited a spherical morphology with a nearly uniform size of 50 nm. The PX-phase PT nanowires exhibited acicular morphology with diameter sizes of 40–60 nm and length up to several micrometers, and the aspect ratio was close to 90. They tended to grow into a regular structure with parallel arrangement along their long axis in the [001] direction. The extinction rule for the diffraction indexes (h, k, l) in the XRD pattern is the sum of (h, k, l) equal to odd number, similar to body-centered cubic crystal. In the SAED patterns of the PX-phase PT nanowires, both super electron diffraction spots with a threefold modulated periodicity along the [110] direction and the appearance of strong diffraction spot (008) but the forbidden (004) spot, were clearly observed, which indicated that the PX-phase PT has a threefold modulated periodicity along the [110] direction, and fourfold modulated periodicity in the [001] direction, respectively. This result was confirmed by high-resolution transmission electron microscopy images. The Raman bands centered near 146, 193, and 292 cm⁻¹ observed in the nanowires at room temperature, could be assigned to the $E(1LO)$, $E(2TO)$, and $E+B_1$ phonon modes of the tetragonal PT structure, respectively. However, no phonon modes of the tetragonal PT structure were responsible for the additional three Raman bands centered near 175, 548, and 832 cm⁻¹, which are presumed to be resulted from the additional Raman modes of the PX-phase PT with a large and complex unit cell.

I. Introduction

RESEARCH and technology of functional ceramics are predominantly focused on perovskite metal oxides with compositions mainly based on BaTiO₃ (BT), PbTiO₃ (PT), and Pb(Zr,Ti)O₃ (PZT). These perovskite compounds readily form solid solutions with a large number of other oxides, thus, provide an immense variety of ferroelectric properties.¹ Ferroelectric materials are characterized by two features, namely, the existence of spontaneous polarization and the possibility to

reorient the polarization by an external electric field. Such prominent features make the ferroelectric oxides possess broad range of properties, such as spontaneous polarization, high dielectric permittivity, piezoelectricity as well as pyroelectricity, which find a variety of applications in nonvolatile ferroelectric memories, thin-film capacitors, piezoelectric sensors and actuators, and pyroelectric detectors.² For example, BT is widely used as dielectric in ceramic capacitors and, in particular, in multilayer ceramic capacitors (MLCCs) because of its high dielectric characteristics. Following a similar trend to miniaturization as conventional semiconductors, the down-sized electronic devices, based on electroceramic materials such as MLCCs, have been developed. In order to enhance the capacitance per unit volume, currently, much effort is focused on increasing the dielectric constant of the ceramic material as well as on decreasing the thickness of the dielectric layers in MLCCs. To achieve a thinner dielectric layer, dielectric BT materials with ultra-fine grains are highly required. At present, the dielectric layer thickness for an MLCC with the highest volumetric efficiency is as thin as 1 μm, and this thickness is expected to become <0.3–0.5 μm within the next 10 years. Consequently, the sizes of BT particles used for fabricating the next generation of MLCCs will be lowered down to tens of nanometers. Although the bulk properties of BT ceramics have been widely investigated, more recently, there has been renewed interest in nanoscale particles of this material because the electrical properties are strongly dependent on the grain size and crystalline structure. Because the tetragonal BT is used in ferroelectrics and cubic BT is used in capacitors a better understanding of the nanostructure of ultrafine BT particles of both phases is of interest as well as the correlation of properties with particle size.

Conventionally, perovskite BT nanoparticles are synthesized by solid-state reactions between barium carbonate and titanium oxides at elevated temperatures above 1000°C.^{3,4} However, the resulting microstructures of the BT powders obtained from this method are not suitable for developing high volume efficient MLCCs, due to their significant particle agglomeration, poor chemical homogeneity, and coarse large particle sizes. In recent years, wet-chemical methods such as the sol–gel method,^{5,6} alkoxide synthesis,^{7,8} and hydrothermal method^{9–12} have been developed to replace the conventional solid-state reactions for the synthesis of perovskite BT nanoparticles. Nanosized BT particles are synthesized by wet-chemical methods, which makes the BaTiO₃ system very attractive for developing new electronic nanodevices. As an example, the synthesis, processing, and electrical characterization of thin (<100 nm thick) nanostructured BT thin films built from uniform BT spherical nanoparticles with a diameter below 20 nm, are reported.¹³ The results show that the BT nanoparticles can be used as initial building blocks for preparation of thin films which exhibit highly uniform nanostructured texture and grain sizes.

Among the chemical methods developed so far, the hydrothermal method is one of the most promising routes for producing extremely fine particles with spherical morphology and narrow size distribution.¹⁴ Perovskite BT nanoparticles synthesized via hydrothermal method have been investigated exten-

R. Riman—contributing editor

Manuscript No. 24165. Received December 30, 2007; approved April 11, 2008.

This work is supported by Natural Science Foundation of Jiangsu Province (Project No. BK2007130), National Found for Fostering Talents of Basic Science (NFFTBS) (Project No. J0630316), and opening key project of National Laboratory of Solid State Microstructures (Z010804), Nanjing University, China.

[†]Author to whom correspondence should be addressed. e-mail: xhzhu1967@yahoo.com.cn

sively with a focus on the MLCCs. The recent significant progresses made in this subject are comprehensively reviewed by Pithan *et al.*,¹⁵ and Yoon and Lee.^{16,17} To control the growth of BT nanoparticles with the desired particle size and morphology, the reaction kinetics and formation mechanisms of BT nanoparticles under hydrothermal conditions have been investigated, and also controversially discussed in the literatures.^{10,14,18–20}

To enhance the crystallization kinetics of hydrothermal process and obtain BT powders with a high degree of homogeneity and uniform particle size at lower temperature, microwave-hydrothermal process, has received much attention due to its many distinct advantages over the conventional hydrothermal process. For example, in the microwave-hydrothermal process, the microwave radiation couples with the material, and the electromagnetic energy is converted into thermal energy, which is absorbed by the material. Therefore, the heat is generated from inside the material, in contrast with conventional autoclave heating methods where the heat is transferred from outside to inside. This internal heat allows very rapid heating to the crystallization temperature, faster kinetics of crystallization by one-to-two orders of magnitude compared with the conventional hydrothermal process, and also saves energy and time. In addition, microwave heating is particularly suitable for perovskite dielectric ceramic materials because the absorption degree of microwaves by them is much high due to their large dielectric constant and high dielectric loss.²¹ BT nanoparticles synthesized under microwave irradiation have been reported^{22–25}; however, the produced BT particles reported previously, usually have a large degree of agglomeration, and varied distributions of particle size and shape. Therefore, much effort remains to be made to synthesize pure-phase BT nanoparticles with uniform fine particle size and spherical morphology by microwave-hydrothermal process for developing high volume efficient MLCCs.

PT is another important ferroelectric material with a perovskite structure and a Curie temperature of 490°C, which is widely applied in electronics as multilayer capacitors, nonvolatile memories, ultrasonic transducers, and pyroelectric detectors, due to a large pyroelectric coefficient and a relatively low permittivity.²⁶ Over the past decade, many chemical methods (e.g., sol-gel,²⁷ coprecipitation,²⁸ combined polymerization and pyrolysis of metallo-organic precursors,²⁹ and hydrothermal^{30–32}) have been developed to prepare the PT powders with controlled physical and chemical characteristics. The crystalline PT powders synthesized via hydrothermal process do not require high temperature calcination process, so the resulting aggregation and the subsequent milling process can be eliminated. Previous works have demonstrated that the PT powders prepared via hydrothermal process exhibit different crystal structures such as perovskite type, pyrochlore type, and tetragonal body-centered type (also named as PX-phase), and various morphologies (e.g., spherical, tabular, and acicular), which are dependent upon the reaction conditions.^{33,34}

Recently, one-dimensional (1D) ferroelectric nanostructures have attracted a great attention due to their distinctive geometries, novel physical and chemical properties, and potential applications in nanodevices. The acicular PX-phase PT nanowires with high aspect ratio, are ideal initial building blocks for fabricating 1D ferroelectric nanostructures, due to their special geometry and anisotropic ferroelectric properties. Suzuki *et al.*³³ have reported on the acicular PX-phase PT nanowires synthesized via hydrothermal method by using TiCl_4 and $\text{Pb}(\text{CH}_3\text{COO})_2$ as starting materials, and KOH as a mineralizer. However, they did not obtain the pure phase of acicular PT nanowires. Later, Cheng *et al.*³⁴ reported the preferable conditions for obtaining pure acicular PT nanowires with aspect ratio over 10 (axis diameter usually < 100 nm and length > 1 μm) by using hydrothermal process and, lead nitrate and titanium butoxide as starting materials. More recently, perovskite PZT crystallites with acicular morphology (diameter of the crystallites < 100 nm and length > 2 μm), synthesized via hydrothermal process by using tetramethylammonium hydroxide pentahy-

drate as a mineralizer, are also reported by Cho *et al.*³⁵ Although the synthesis of acicular PX-phase PT nanowires has been reported, however, their chemical formula $(\text{PbTiO}_3)_n$ (n —an unknown integer), and crystal structures, still remain unclear due to the lack of high-resolution transmission electron microscopy (HR-TEM) characterizations of these anisotropic nanowires. Clearly, to better understand the microstructure of PX-phase PT nanowires at atomic scale, much HR-TEM work remains to be done.

The objective of the current work is given an effort to synthesize high pure, agglomerate-free perovskite BT nanoparticles with spherical morphology and monodispersed sizes by microwave-hydrothermal process at temperatures as low as 150°C, and their atomic-scale microstructures were characterized by electron microscopy. In addition, the PX-phase acicular PT nanowires with aspect ratio close to 90, synthesized via microwave-hydrothermal method, are also characterized by HR-TEM at atomic scale for the first time, to the knowledge of the authors. Our new findings reveal that the PX-phase PT nanowires have a threefold modulated periodicity along the [110] direction, and fourfold modulated periodicity in the [001] direction. They tend to grow into a regular structure with parallel arrangement along their long axis in the [001] direction. The Raman spectroscopy study of the nanowires at room temperature also demonstrates that some additional Raman modes are produced in the large and complicated unit cell of PX-phase PbTiO_3 .

II. Experimental Procedure

(1) Starting Materials

Reagents of lead acetic hydrate ($\text{Pb}(\text{CH}_3\text{COO})_2 \cdot 3\text{H}_2\text{O}$) (Sigma Aldrich, Shanghai, China), barium chloride ($\text{BaCl}_2 \cdot 2\text{H}_2\text{O}$) (Sigma Aldrich), and tetrabutyl titanium ($\text{Ti}(\text{OC}_4\text{H}_9)_4$) (Sigma Aldrich) were used as lead, barium, and titanium sources. Potassium hydroxide (KOH) (Sigma Aldrich) was used as alkaline mineralizer.

(2) Microwave-Hydrothermal Synthesis

All the syntheses were performed using the MARS 5 (CEM Corp., Matthews, NC) microwave digestion system. The system was operated at a 2.45 GHz with a maximum power of 1200 W, and the power varied from 0% to 100%. The system was controlled by temperature (maximum, 300°C) and pressure (maximum, 800 psi). The adjusted parameters were pressure/temperature, power, and hold time. The syntheses were carried out in double-walled digestion vessels, which has an inner liner and cover made up of Teflon PFA and outer high strength vessel shell made of Ultem polyetherimide. For a typical synthesis of BT nanoparticles, 1.1217 g · mol of KOH was dissolved in 20 mL of boiled double-distilled water followed by addition of 0.7808 g of $\text{BaCl}_2 \cdot 2\text{H}_2\text{O}$ and 0.5 mL $\text{Ti}(\text{OC}_4\text{H}_9)_4$. Boiled double-distilled water was used to minimize the carbonate content of the crystallized powder. The pH value of the resultant mixture was found to be 14.0. The reaction mixture was heated to the temperature of 150°C at a heating ramp of 5°C/min and maintained at that temperature for 50 min. After reaction, the autoclave was cooled down to room temperature, and the crystallized BaTiO_3 powders were separated by centrifugation and repeatedly washed with 0.1M aqueous nitric acid, filtered and thoroughly washed with distilled water several times, and finally oven-dried at 100°C for 24 h before structural characterizations. To reduce the degree of particle agglomeration and to control the size and morphology of the BT nanoparticles, besides pure water solution, the reactive medium of water-ethylene glycol (EG, Sigma Aldrich) mixed solution with a volume ratio of 1:2, was also used for synthesis of BT nanoparticles under microwave irradiation. For convenience, the produced BT nanoparticles by using pure water as reactive medium were referred to as BT-1 sample, and the BT-2 sample designated for the BT nanoparticles synthesized in a reactive medium of water-EG mixed solution with a volume ratio of 1:2.

The PX-phase PT nanowires with acicular morphology were fabricated via microwave-hydrothermal process, and the typical synthesized process was described as the followings. Initially, high-purity $\text{Pb}(\text{CH}_3\text{COO})_2 \cdot 3\text{H}_2\text{O}$ of 2.50 g was dissolved in de-ionized water and $\text{Ti}(\text{OC}_4\text{H}_9)_4$ of 1.80 g was dissolved in ethanol to form a uniform solution by stirring, respectively. And then the solution containing $\text{Ti}(\text{OC}_4\text{H}_9)_4$ was slowly introduced into the solution containing $\text{Pb}(\text{CH}_3\text{COO})_2 \cdot 3\text{H}_2\text{O}$ while stirring slightly by a glass bar, and the pH value of the mixed solution was adjusted to 13.0 by adding KOH. The mixture was then transferred to an autoclave (filled up to about 80% capacity) where it was immediately sealed and placed in a microwave oven. The microwave-hydrothermal reactions of PX-phase PT nanowires were carried out at 200°C for 90 min in an oven. After cooling down to room temperature, the obtained products were washed with organic acids and distilled water for several times, to remove the absorbed impurities. Finally the nanowires were dried at 80°C in an oven for 24 h before microstructural characterization.

(3) Structural Characterization

The crystal structure and phase composition of the synthesized BT nanoparticles and PX-phase PT nanowires were structurally characterized by X-ray diffraction (XRD, Philips X'Pert MRD four-circle diffractometer, Almelo, the Netherlands) using $\text{CuK}\alpha$ radiation, and by scanning at 0.01°/s. Raman scattering investigations of the PX-phase PT nanowires were performed at room temperature with a Jobin Yvon HR800 spectrometer (JY Ltd., Horiba, France) with visible laser light (wavelength 514.5 nm) as the excitation source. The slits were adjusted so that the resolution was 1 cm^{-1} . The morphology and microstructure of BT nanoparticles and PT nanowires were examined by Philips CM20 TEM (operated at 200 kV), HR-TEM (JEM-4000EX, JEOL Ltd., Tokyo, Japan) and selected area electron diffraction (SAED). The TEM, HR-TEM images, and SAED patterns were recorded by Gatan multiscan charge-coupled device (CCD) camera system (Model 794, Gatan Inc., Pleasanton, CA). The TEM specimens were prepared by dispersing the BT powders or the PT nanowires in ethanol, mixing it in an ultrasonic generator, and putting a droplet of this dispersion on a copper grid with a supported carbon thin film. The fast Fourier transform (FFT) pattern and the corresponding Fourier filtered HR-TEM images were obtained by using the Gatan Digital Micrography software (revised version 2.0, Gatan Inc.).

III. Results and Discussion

(1) BaTiO_3 Nanoparticles

XRD patterns of the BT nanoparticles from the BT-1 sample synthesized by microwave-hydrothermal process in a reactive medium of pure water, before and after washed by nitric acid, are shown in Fig. 1(A). It is observed that all the peaks fit well to the peak positions of cubic phase BT (JCPDS No.31-174). Normally, the diffraction pattern at the $2\theta \approx 45^\circ$ region is a characteristics of the presence of either cubic or tetragonal BT phase structure. In this case, no splitting of cubic (200) into tetragonal (200) and (002) reflections at about 45° , can be observed. To demonstrate this clearly, a local fine XRD pattern scanned at 2θ in the range of 44° – 46° , is shown as an inset in Fig. 1(A). Actually, only a singlet XRD peak was observed at $2\theta \approx 45^\circ$ (diffraction peak from (200) plane). This indicates that the particles from BT-1 sample are of perovskite cubic structure at room temperature. This result is also confirmed by the following SAED patterns. It is also noticed that a weak diffraction peak appears at about $2\theta \approx 22^\circ$ in the BT-1 sample (without washing by nitric acid), which was resulted from BaCO_3 by-product (JCPDS No.11-697, in which, the diffraction peak (111) is positioned at $2\theta \approx 22.09^\circ$). The BaCO_3 impurity is probably formed by the dissolution of atmospheric CO_2 in the alkaline solution, and followed by the precipitation of insoluble BaCO_3 . However, this impurity can be completely removed by washing the pro-

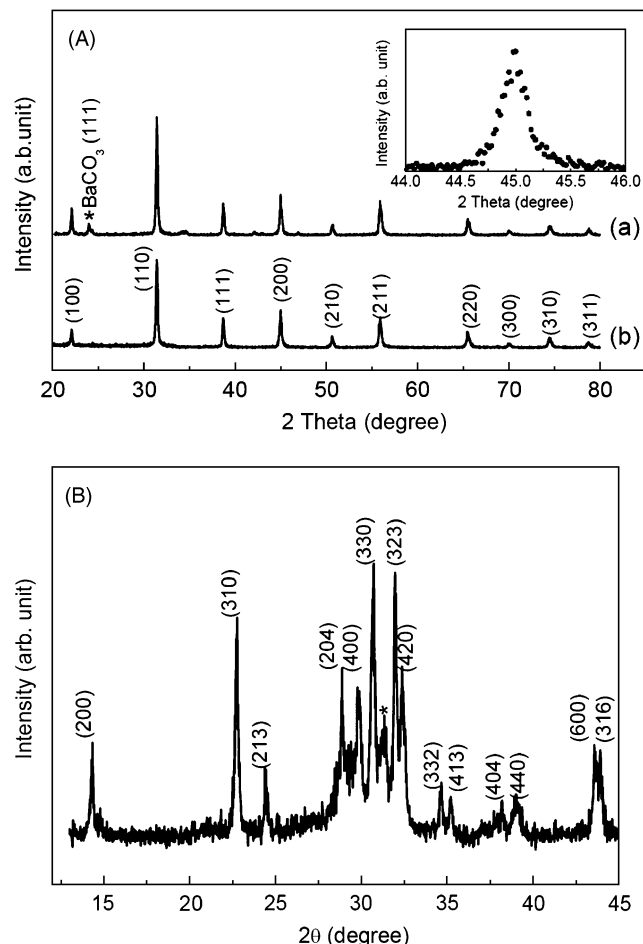


Fig. 1. X-ray diffraction (XRD) patterns of (A) nanoparticles from sample BaTiO_3 (BT)-1 and (B) acicular PT nanowires, synthesized by microwave-hydrothermal process in reactive medium of pure water. In (A), (a) and (b) are the XRD patterns of the BT-1 samples before and after washed by nitric acid, respectively. The inset in (A) shows a local fine XRD pattern scanned at 2θ from 44° to 46° .

duced powders with aqueous nitric acid, as confirmed by the comparison of the two XRD patterns shown in Fig. 1(A).

The grain sizes and morphologies of the nanoparticles from BT-1 and BT-2 samples were revealed by TEM images, as shown in Figs. 2(A) and (B), respectively. It is clearly observed that in Fig. 2(A) many BT nanoparticles with sizes of 85–105 nm, have a strong tendency to agglomerate together, forming the agglomerates with sizes of 170–260 nm. It is reported that the basic forces responsible for agglomeration process are the van der Waals forces of attraction.³⁶ If van der Waals attractive forces dominate over the repulsive forces at all distances, the nanoparticles will agglomerate. Owing to the Brownian motion, the nanoparticles may become in contact and agglomerate, as the primary nanoparticles are colloidal in nature. Larger particles may get settled down under the influence of gravitational force to form agglomerates. All the above-mentioned processes can contribute to the formation of agglomerates and the reduction of surface energies of nanoparticles.

In the BT-2 sample, the reactive medium for microwave-hydrothermal process was water-EG mixed solution with a volume ratio of 1:2. It is observed that in Fig. 2(B) the BT nanoparticles have nearly uniform size (~ 50 nm) and spherical morphology. In comparison with BT-1 sample, BT-2 sample has smaller particle size and better monodispersibility and crystallinity. The possible reasons for the formation of nearly monodispersed nanoparticles in BT-2 sample are described below.

In the microwave-hydrothermal process, the formation mechanism of nearly monodisperse BT nanoparticles with

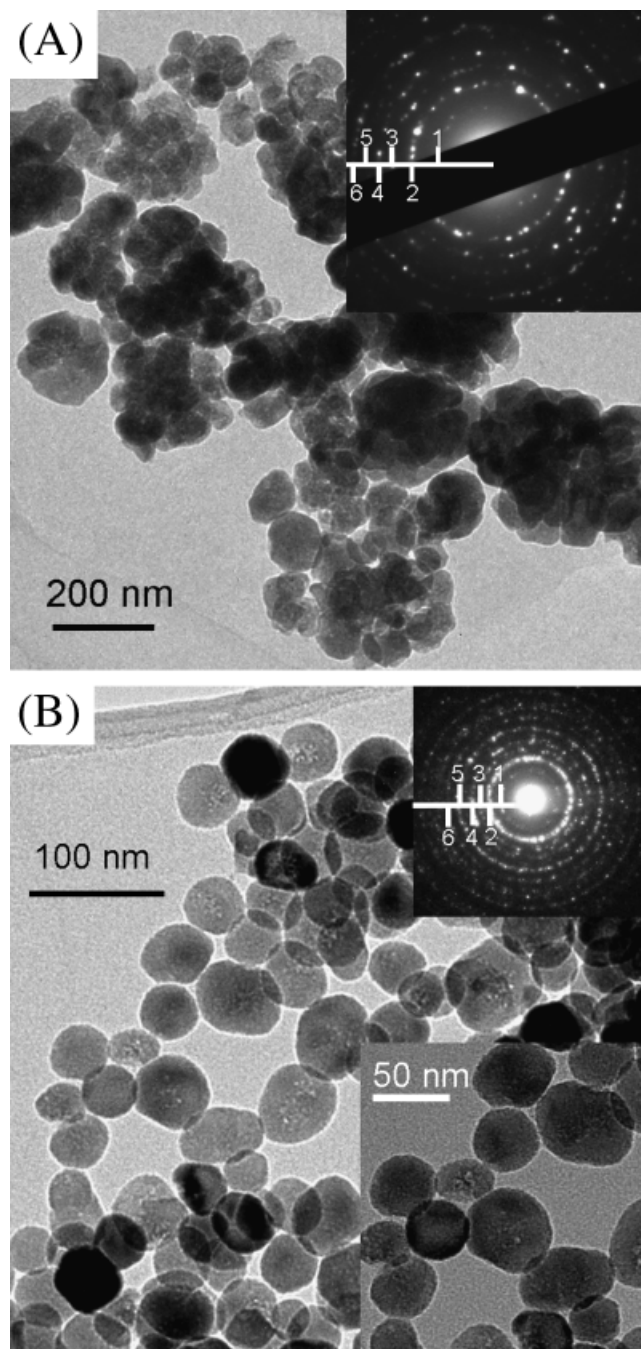


Fig. 2. Bright-field transmission electron microscopy (BF-TEM) images of BaTiO₃ (BT) nanoparticles from (A) BT-1 and (B) BT-2 samples. Two insets at the top-right corners are the selected area electron diffraction patterns taken from the BT-1 and BT-2 samples, respectively. The first six diffraction rings marked in the insets can be labeled as (100), (110), (111), (200), (210), and (211), respectively. The inset at the bottom-right corner in B, is an enlarged TEM of the BT nanoparticles from the BT-2 sample.

spherical morphology is proposed to involve different growth process. First is the initial nucleation, and then the growth of BT nanoparticles following a classical growth model,³⁷ and eventually aggregation into larger units following with other growth kinetics like the Smoluchowski's equation.³⁸ For the formation of spherical nanoparticles, there must exist sufficient short-range repulsion between the nucleates in the highly basic environment, to restrict them forming agglomerations. The presence of EG solvent in the reactive medium can serve as surfactants, which surrounds at the surface of the forming BT nucleates, providing a barrier against the agglomeration and overgrowth of BT nanoparticles through the microreactors

formed by the EG solvent. An increase of the viscosity of the reactive medium caused by the presence of EG solvent was also noticed, which might also influence the size and morphology of the nucleated nanoparticles. While we have not yet obtained the systematic data of the viscosity values related to the particle morphologies, however, in comparison with the BT-1 sample, the growth of the nanoparticles in BT-2 sample was apparently restrained by the presence of EG solvent in the reactive medium. This finding is in agreement with the observations reported by other researches in synthesizing BT nanoparticles by alcohol-thermal process.^{38,39} The control of particle morphology in a solution particle synthesis is a complex process requiring a fundamental understanding of the interactions between solid-state chemistry, interfacial reactions and kinetics, and solution chemistry. In particular, the microwave-hydrothermal process conducted under microwave irradiation and high pressure in a closed reaction vessel, usually makes it much more difficult to identify the solution species and, subsequently, to control, much less predict, the particle shapes produced. However, in the present work, the EG solvent was used as surfactant to form microreactors in the reactive medium, controlling the size and morphology of the BT nanoparticles. By this way, perovskite cubic BT nanoparticles with nearly uniform size of 50 nm and spherical morphology were synthesized, which have promising applications in the next generation of high volume efficient MLCCs, where the particle sizes of the BT raw materials are required to be only a few tens of nanometers with spherical morphology. A systematic study of the influence of EG solvent on the size and morphology of BT nanoparticles synthesized by microwave-hydrothermal process, is currently in progress and will be reported in a separate article.

The insets shown in Figs. 2(A) and (B) are the SAED patterns taken from the BT-1 and BT-2 samples, which show polycrystalline diffraction rings consisting of discrete diffraction spots. The first six diffraction rings are indicated in the two SAED patterns. The diameters (D_i , $i = 1-6$) of the first six diffraction rings were measured and the D_i^2/D_1^2 ratios ($i = 1-6$) were also calculated. It was found that the D_i^2 ratios are equal to 1:2:3:4:5:6. That means the SAED patterns are consistent with the particles being of the BaTiO₃ phase, and the diffraction rings correspond well to the cubic perovskite structure. This result is in well agreement with the above XRD. The first six diffraction rings can be indexed as (100), (110), (111), (200), (210), and (211), respectively.

The BT nanoparticles are also found to be single crystalline, as additionally proven by high-resolution lattice images of individual particles. Figure 3(A) is an HR-TEM image of the interface between two adjacent BT nanoparticles from the BT-1 sample. The lattice fringes are clearly observed in the two BT nanoparticles. Their interplanar spacing was measured to be 0.405 nm, which corresponds to the {100} lattice spacing of BT. Figure 3(B) is a HR-TEM image of a nanoparticle from BT-2 sample. This particle is oriented along the [001] axis, and 2D lattice fringes for the two perpendicular sets of (100) and (010) planes are clearly observed. The insets shown in Fig. 3(B) are the Fourier filtered HR-TEM image and the FFT pattern of the nanoparticle. The sharp reflections of the FFT pattern can be unambiguously attributed to the BT structure for a particle oriented along the [001] direction. It is clearly observed that the lattice fringes in the Fourier filtered HR-TEM image have some degree of distortion, indicating some strains within the nanoparticle.

(2) Acicular PbTiO₃ Nanowires

XRD pattern of the acicular PT powders synthesized by microwave-hydrothermal process is shown in Fig. 1(B). It is observed that all the diffraction peaks can be indexed as the PX-phase PbTiO₃ (JCPDS card no.48-0105), except for a small diffraction peak marked with an asterisk at $2\theta = 31.33^\circ$, which was found out to be the (101) peak of tetragonal PbTiO₃ (JCPDS No.75-0438, in which, the (101) diffraction peak is positioned at

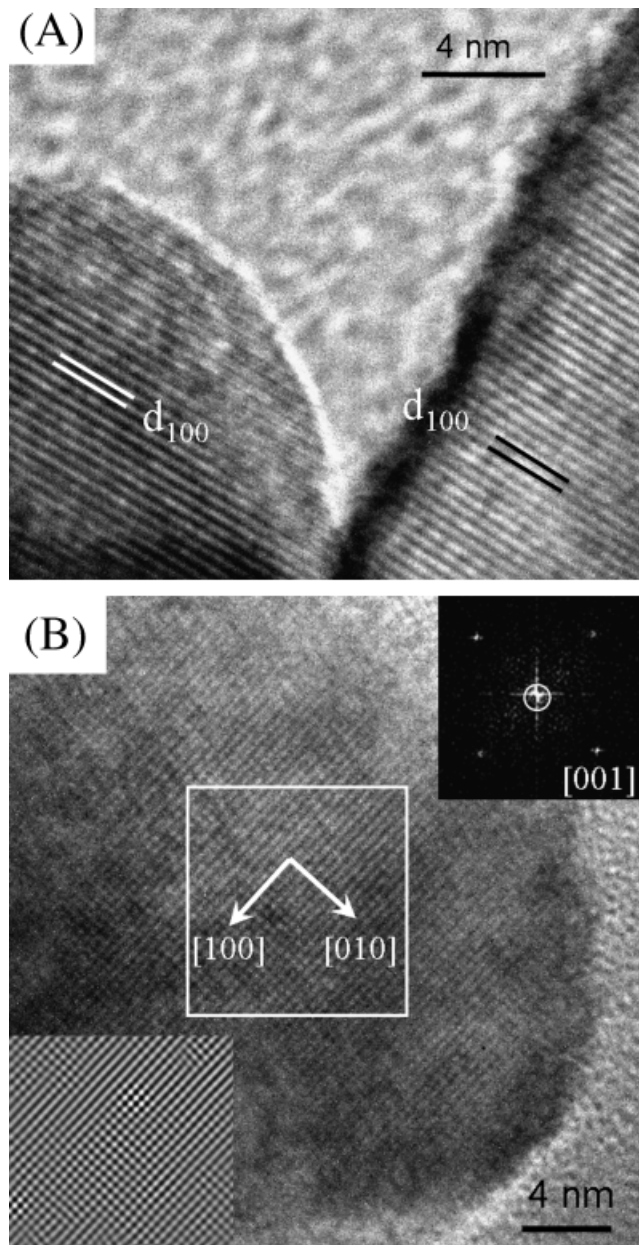


Fig. 3. (A) A high-resolution transmission electron microscopy (HR-TEM) image of the interface between two adjacent nanocrystalline BaTiO_3 (BT) particles observed in the BT-1 sample, and (B) a profile HR-TEM image of a nanoparticle from the BT-2 sample viewed from [001] direction. The two insets in B are the Fourier filtered HR-TEM image and the fast Fourier pattern of the nanoparticle, respectively.

$2\theta = 31.32^\circ$). The unit cell parameters of the acicular PT nanowires were calculated as $a = 12.33 \text{ \AA}$ and $c = 14.49 \text{ \AA}$, matching well with the literature values of $a = 12.358 \text{ \AA}$ and $c = 14.541 \text{ \AA}$.³⁴ It is also noticed that the forbidden diffraction indexes of the acicular PX-phase PT nanowires, follow with a rule that the sum of diffraction indexes (h, k, l) is odd number, similar to the case of body-centered cubic crystal.

To obtain the information on the crystal structure of the acicular nanowires from vibrational spectra, Raman scattering investigations were also performed in this work. Figure 4 illustrates the Raman spectrum of the produced acicular PT nanowires. Six characteristic major Raman bands centered near 146, 175, 193, 292, 548, and 832 cm^{-1} , are clearly observed. Among them, the Raman bands centered near 146, 193, and 292 cm^{-1} can be assigned to the $E(1\text{LO})$, $E(2\text{TO})$, and $E+B_1$ phonon modes of the tetragonal PbTiO_3 structure, respectively. However, no phonon modes of the tetragonal PbTiO_3 could

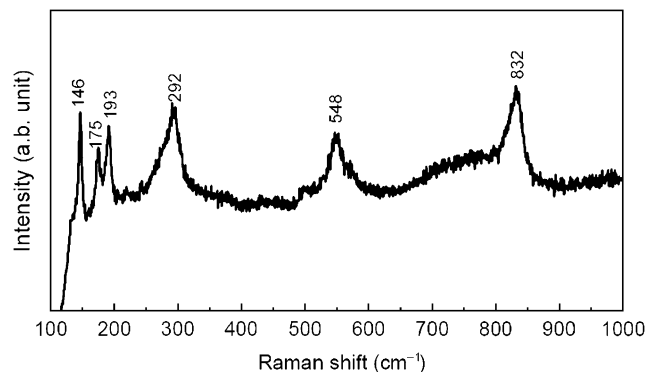


Fig. 4. Raman spectroscopy of the produced acicular PX-phase PT nanowires.

be responsible for the observed Raman bands around 175, 548, and 832 cm^{-1} . These Raman bands are presumed to be resulted from the additional Raman modes of the PX-phase PbTiO_3 with a large and complicated unit cell. It is reported that the distortions of the oxygen octahedra, B-type cation displacement within the octahedra, and the tilting of the octahedra relative to one another as rigid corner-linked units, appear in a more complex perovskite-derived structure,⁴⁰ they can break the translational symmetry to some degree, and cause the local electric fields and local polarizability no longer replicating exactly from one unit cell to another, resulting in additional Raman modes of PX-phase PT nanowires.

It is known that the Raman spectra of crystals with relatively small unit cells and a limited number of atoms, usually exhibit all of the Raman modes, as expected from symmetry arguments. However, in a complex unit cell with lots of atoms, experimental results account for fewer and fewer of the calculated Raman modes. The possible reasons may include⁴¹: (1) mode degeneracy (two, three, or more modes are required by crystal symmetry, to have almost the same wavenumber, appearing as a single band in the Raman spectra), (2) some Raman modes are forbidden to be appeared due to symmetry confinements, (3) weak bands lost in the measurement noise, and (4) more low wavenumber bands are produced due to the possible complex torsional motions in a large unit cell like PX-phase PbTiO_3 .

The TEM images of the acicular PT nanowires are shown in Fig. 5. In Fig. 5(A), it can be seen that 2~3 acicular PT nanowires with a diameter of 40 nm, grew in parallel arrangement along their long axes, and the lengths of the wires are over 3 μm .

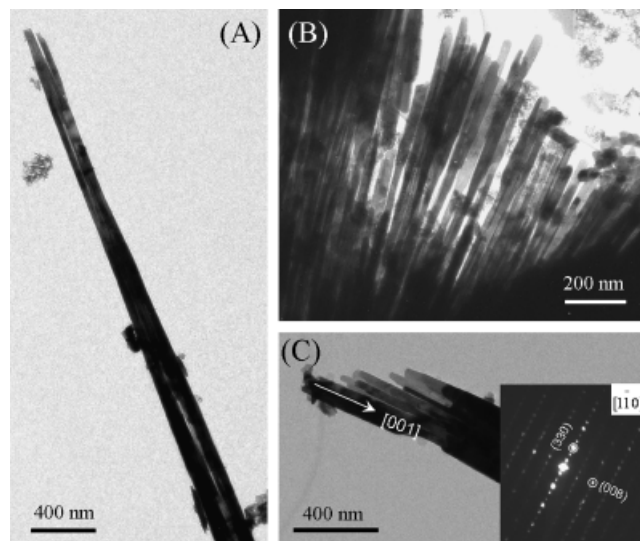


Fig. 5. Transmission electron microscopy images of the acicular PX-phase PT nanowires with average diameter sizes of (A) 40 nm, (B) 50 nm, and (C) 60 nm.

As a consequence, their aspect ratio is close to 90. Such nanowires with a high aspect ratio, used as initial building blocks, will have potential applications in fabricating 1D ferroelectric nanostructures due to their unique geometry and anisotropic ferroelectric properties. In Fig. 5(B), bundles of acicular PT nanowires are also observed, they tend to arrange side by side along their long axes, due to the van der Waals and/or electrostatic attraction forces. The diameter of an individual nanowire is about 50 nm and length usually up to 1 μm . In Fig. 5(C), several 1D acicular PT nanowires grew into a regular structure with parallel arrangement, and the average diameter of the wires is about 60 nm with length up to 2 μm . The SAED pattern (inset of Fig. 5C) shows clear diffraction spots of the crystalline PX-phase PbTiO_3 , which is taken from the $[1\bar{1}0]$ direction. Based on the TEM image and SAED pattern, it can be determined that the long axis of the nanowires is parallel to the $[001]$ direction, and the nanowires grew along the $[001]$ direction, as marked by a white arrow in Fig. 5(C). In addition, the superlattice electron

diffraction spots with a threefold periodicity along the $[110]$ direction are also clearly observed in the SAED pattern, which suggests that in the (001) plane, the PX-phase PbTiO_3 has a modulation with a periodicity of $3d_{600}$ ($= 0.6165$ nm) along the a and b axes, respectively. This result is also confirmed by HR-TEM images. Furthermore, in the $[001]$ direction, the appearance of (008) diffraction spot with strong intensity and the forbidden (004) one are also observed, indicating that the PX-phase PbTiO_3 has a modulation with a periodicity of $4d_{008}$ ($= 0.7245$ nm) along the $[001]$ direction.

The HR-TEM images of the PX-phase PT nanowires are shown in Fig. 6. In Fig. 6(A), well-developed lattice fringes are clearly observed, indicating a good crystallinity of the PX-phase PT nanowires. The lattice fringes of the HR-TEM image were examined to be 0.617 nm, close to the (200) lattice spacing of the PX-phase PT. The inset at right-bottom corner in Fig. 6(A), is an enlarged HR-TEM image of the selected area marked by a box in Fig. 6(A), which clearly demonstrates a modulated structure along the $[100]$ direction. Three sub-layers are observed between two adjacent (200) lattice fringes, and each sub-layer correspond wells to the interplanar distance of (600) plane. Therefore, the PX-phase PbTiO_3 has threefold modulated periodicity along the $[100]$ direction. The FFT pattern of the PX-phase PbTiO_3 nanowires, is shown as an inset in Fig. 6(A) (top-right corner), which demonstrates the periodically modulated structure of PX-phase PbTiO_3 . Similarly, the PX-phase PbTiO_3 also has threefold modulated periodicity along the $[110]$ direction, as revealed by the HR-TEM image shown in Fig. 6(B). The (110) lattice fringes of the PX-phase PT are clearly observed, and in the enlarged HR-TEM image of the selected area, the (330) lattice fringes are also clearly observed, as marked by dot lines. The inset in Fig. 6(B) at top-right corner, is the corresponding FFT pattern of the HR-TEM image, which reflects the modulated structure of the PX-phase PbTiO_3 along the $[110]$ direction. That agrees well with the results obtained from the above SAED pattern.

IV. Conclusions

In summary, we report on the syntheses of pure perovskite spherical BaTiO_3 nanoparticles and acicular PbTiO_3 (PX-phase) nanowires by microwave-hydrothermal method, and their microstructures are investigated at atomic-scale by electron microscopy. The results showed that the produced BT nanoparticles with spherical morphology and nearly uniform size of 50 nm, remained a metastable cubic perovskite structure at room temperature. The PX-phase PT nanowires with acicular morphology tended to grow into a regular structure with parallel arrangement along their long axis in the $[001]$ direction. Their diameter sizes were in the range of 40–60 nm with axial length up to several micrometers. Such nanowires with high aspect ratio of 90, are ideal initial building blocks for constructing 1D ferroelectric nanostructures, due to their special geometry and anisotropic ferroelectric properties. The forbidden diffraction indexes in the diffraction patterns of the acicular PT nanowires followed with a rule of the sum of diffraction indexes (h, k, l) with odd number. The SAED patterns revealed that the superlattice electron diffraction spots had a threefold modulated periodicity along the $[110]$ direction, whereas a fourfold modulated periodicity in the $[001]$ direction. This result was confirmed by the HR-TEM images. Six characteristic major Raman bands centered near 146, 175, 193, 292, 548, and 832 cm^{-1} , were clearly observed in the Raman spectrum of the acicular PX-phase PbTiO_3 nanowires. Among them, the Raman bands centered near 146, 193, and 292 cm^{-1} could be assigned to the $E(1\text{LO})$, $E(2\text{TO})$, and $E+B_1$ phonon modes of the tetragonal PbTiO_3 , respectively. However, no phonon modes of tetragonal PbTiO_3 could be responsible for the additional three Raman bands around 175, 548, and 832 cm^{-1} . These Raman bands are presumed to be resulted from the additional Raman modes of the PX-phase PbTiO_3 , because the complex torsional motions of the

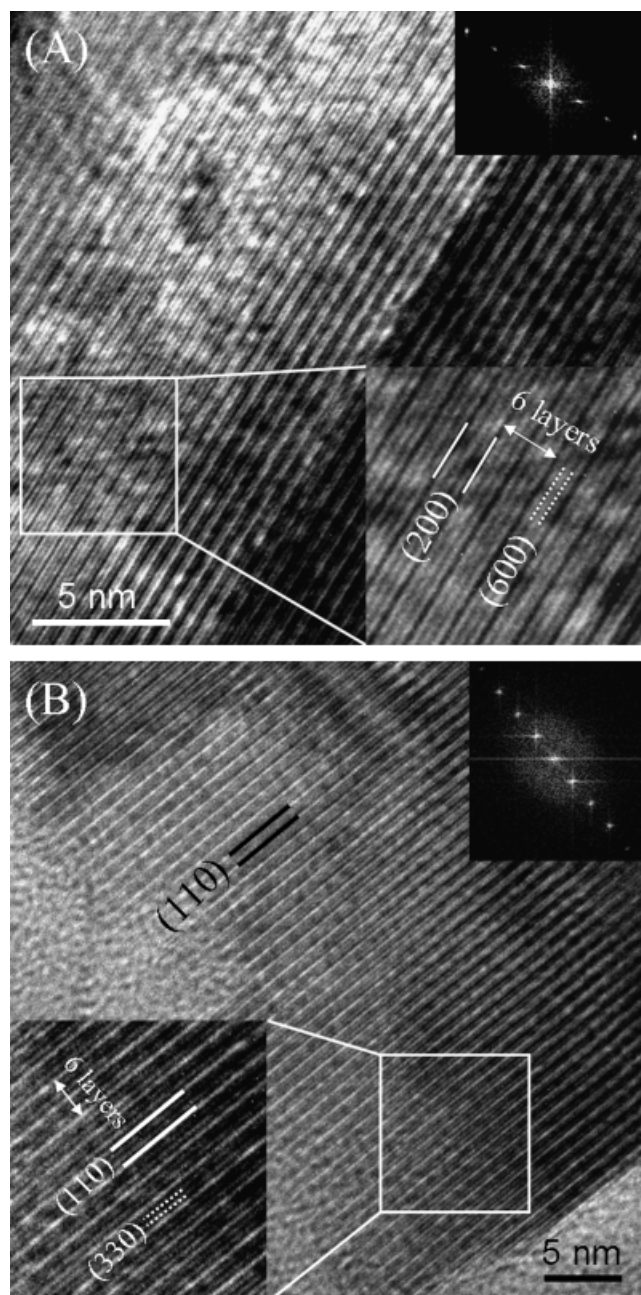


Fig. 6. High-resolution transmission electron microscopy images of the acicular PX-phase PT nanowires, showing the threefold modulated periodicity along (A) $[100]$ and (B) $[110]$ directions, respectively.

oxygen octahedral are possible in the super unit cell of the PX-phase PbTiO_3 , which could lead to additional Raman modes.

References

- ¹M. E. Lines and A. M. Glass, *Principles and Applications of Ferroelectrics and Related Materials*, Oxford University Press, Oxford, U.K., 2001.
- ²G. H. Haertling, "Ferroelectric Ceramics: History and Technology," *J. Am. Ceram. Soc.*, **82**, 797–818 (1999).
- ³M. S. H. Chu and A. W. I. M. Rae, "Manufacturing Dielectric Powders," *Am. Ceram. Soc. Bull.*, **74**, 69–74 (1995).
- ⁴A. Beauger, J. C. Mutin, and J. C. Niepce, "Synthesis Reaction of BaTiO_3 : Part 2 Study of Solid-State Reaction Interfaces," *J. Mater. Sci.*, **18**, 3543–50 (1983).
- ⁵P. P. Phule and S. H. Risbud, "Sol–Gel Synthesis of BaTiO_3 Powders Using Barium Acetate and Titanium Isopropoxide," *Adv. Ceram. Mater.*, **3**, 183–5 (1988).
- ⁶C. Lemoine, B. Gilbert, B. Michaux, J. P. Pirard, and A. J. Lecloux, "Synthesis of Barium Titanate by the Sol–Gel Process," *J. Non-Cryst. Solids*, **175** [1] 1–13 (1994).
- ⁷M. H. Frey and D. A. Payne, "Synthesis and Processing of Barium Titanate Ceramics from Alkoxide Solutions and Monolithic Gels," *Chem. Mater.*, **7** [1] 123–9 (1995).
- ⁸F. Chaput and J.-P. Boilot, "Alkoxide-Hydroxide Route to Synthesize BaTiO_3 -Based Powders," *J. Am. Ceram. Soc.*, **73** [4] 942–8 (1990).
- ⁹S. Yoon, S. Baik, M. G. Kim, N. Shin, and I. Kim, "Synthesis of Tetragonal Barium Titanate Nanoparticles Via Alkoxide–Hydroxide Sol–Precipitation: Effect of Water Addition," *J. Am. Ceram. Soc.*, **90** [1] 311–4 (2007).
- ¹⁰J. O. Jr. Eckert, C. C. Hung-Houston, B. L. Gersten, M. M. Lencka, and R. E. Riman, "Kinetics and Mechanisms of Hydrothermal Synthesis of Barium Titanate," *J. Am. Ceram. Soc.*, **79** [11] 2929–39 (1996).
- ¹¹I. J. Clark, T. Takeuchi, N. Ohtori, and D. C. Sinclair, "Hydrothermal Synthesis and Characterization of BaTiO_3 Fine Powders: Precursors, Polymorphism and Properties," *J. Mater. Chem.*, **9** [1] 83–91 (1999).
- ¹²E. Ciftci, M. N. Rahaman, and M. Shumsky, "Hydrothermal Precipitation and Characterization of Nanocrystalline BaTiO_3 Particles," *J. Mater. Sci.*, **36**, 4875–82 (2001).
- ¹³L. Huang, Z. Y. Chen, J. D. Wilson, S. Banerjee, R. D. Robinson, I. P. Herman, R. Laibowitz, and S. O'Brien, "Barium Titanate Nanocrystals and Nanocrystal Thin Films: Synthesis, Ferroelectricity, and Dielectric Properties," *J. Appl. Phys.*, **100** [3] 034316 (2006), 10pp.
- ¹⁴R. Vivekanandan and T. R. N. Kutty, "Characterization of Barium Titanate Fine Powders Formed from Hydrothermal Crystallization," *Powder Technol.*, **57**, 181–92 (1989).
- ¹⁵C. Pithan, D. Hennings, and R. Waser, "Progress in the Synthesis of Nanocrystalline BaTiO_3 Powders for MLCC," *Int. J. Appl. Ceram. Technol.*, **2** [1] 1–14 (2005).
- ¹⁶D. H. Yoon, "Tetragonality of Barium Titanate Powder for a Ceramic Capacitor Application," *J. Ceram. Proc. Res.*, **7** [4] 343–54 (2006).
- ¹⁷D. H. Yoon and B. I. Lee, " BaTiO_3 Properties and Powder Characteristics for Ceramic Capacitors," *J. Ceram. Proc. Res.*, **3** [2] 41–7 (2002).
- ¹⁸W. Hertl, "Kinetics of Barium Titanate Synthesis," *J. Am. Ceram. Soc.*, **71** [10] 879–83 (1988).
- ¹⁹B. A. Ovrmenko, L. I. Shvets, F. D. Ovcharenko, and B. Y. Kornilovich, "Kinetics of Hydrothermal Synthesis of Barium Metatitanate," *Izv. Akad. Nauk SSSR Neorg. Mater.*, **15**, 1982–5 (1979).
- ²⁰P. Pinceloup, C. Courtois, J. Vicens, A. Leriche, and B. Thierry, "Evidence of a Dissolution–Precipitation Mechanism in Hydrothermal Synthesis of Barium Titanate Powders," *J. Eur. Ceram. Soc.*, **19**, 973–7 (1999).
- ²¹W. Sutton, "Microwave Processing of Ceramic Materials," *Ceram. Bull.*, **68** [2] 376–86 (1989).
- ²²L. T. Guo, H. J. Luo, J. Q. Gao, L. Z. Guo, and J. F. Yang, "Microwave Hydrothermal Synthesis of Barium Titanate Powders," *Mater. Lett.*, **60**, 3011–4 (2006).
- ²³S. H. Jung, J. H. Lee, J. W. Yoon, Y. K. Hwang, J. S. Hwang, S. E. Park, and J. S. Chang, "Effects of Reaction Conditions in Microwave Synthesis of Nanocrystalline Barium Titanate," *Mater. Lett.*, **58**, 3161–5 (2004).
- ²⁴B. L. Newalkar, S. Komarneni, and H. Katsuki, "Microwave–Hydrothermal Synthesis and Characterization of Barium Titanate Powders," *Mater. Res. Bull.*, **36**, 2347–55 (2001).
- ²⁵Y. Ma, E. Vilenko, S. L. Suib, and P. K. Dutta, "Synthesis of Tetragonal BaTiO_3 by Microwave Heating and Conventional Heating," *Chem. Mater.*, **9**, 3023–31 (1997).
- ²⁶M. Dawber, K. M. Rabe, and J. F. Scott, "Physics of Thin-Film Ferroelectric Oxides," *Rev. Mod. Phys.*, **77**, 1083–130 (2005).
- ²⁷N. Tangboriboon, A. M. Jamieson, A. Sirivat, and S. Wongkasemjit, "A Novel Route to Perovskite Lead Titanate from Lead and Titanium Glycolates Via the Sol–Gel Process," *Appl. Organometal. Chem.*, **20**, 886–94 (2006).
- ²⁸J. Fang, J. Wang, L. M. Gan, S. C. Ng, C. H. Chew, and L. M. Gan, "Preparation and Characterisation of Ultrafine Lead Titanate (PbTiO_3) Powders," *J. Mater. Sci.*, **34**, 1943–53 (1999).
- ²⁹E. Erdem, R. B. Otcher, H. C. Semmelhack, H. J. G. Lasel, E. Hartmann, and D. Hirsch, "Preparation of Lead Titanate Ultrafine Powders from Combined Polymerisation and Pyrolysis Route," *J. Mater. Sci.*, **38**, 3211–7 (2003).
- ³⁰S. B. Cho, J. S. Noh, M. M. Lencka, and R. E. Riman, "Low Temperature Hydrothermal Synthesis and Formation Mechanisms of Lead Titanate (PbTiO_3) Particles Using Tetramethylammonium Hydroxide: Thermodynamic Modeling and Experimental Verification," *J. Eur. Ceram. Soc.*, **23**, 2323–35 (2003).
- ³¹M. C. Gelabert, B. L. Gersten, and R. E. Riman, "Hydrothermal Synthesis of Lead Titanate from Complexed Precursor Solutions," *J. Cryst. Growth*, **211**, 497–500 (2000).
- ³²G. Z. Wang, R. Sæterli, P. M. Rørvik, A. T. J. van Helvoort, R. Holmestad, T. Grande, and M. A. Einarsrud, "Self-Assembled Growth of PbTiO_3 Nanoparticles into Microspheres and Bur-Like Structures," *Chem. Mater.*, **19**, 2213–21 (2007).
- ³³M. Suzuki, S. Uedaira, H. Masuya, and H. Tamura, "Hydrothermal Synthesis of Lead Titanate Fine Powders"; pp. 163–70 in *Ceramic Transactions, Vol. 1, Ceramic Powder Science II*, Edited by G. L. Messing, American Ceramic Society, Westerville, OH, 1998.
- ³⁴H. Cheng, J. M. Ma, Z. G. Zhao, D. Qiang, Y. X. Li, and X. Yao, "Hydrothermal Synthesis of Acicular Lead Titanate Fine Powders," *J. Am. Ceram. Soc.*, **75** [5] 1123–8 (1992).
- ³⁵S. B. Cho, M. Oledzka, and R. E. Riman, "Hydrothermal Synthesis of Acicular Lead Zirconate Titanate (PZT)," *J. Cryst. Growth*, **226**, 313–26 (2001).
- ³⁶V. K. LaMer and R. H. Dinegar, "Theory, Production and Mechanism of Formation of Monodispersed Hydrosols," *J. Am. Chem. Soc.*, **72** [11] 4847–54 (1950).
- ³⁷C. J. Brinker and G. W. Scherer, *Sol–Gel Science: The Physics and Chemistry of Sol–Gel Processing*, Academic, London, 1990.
- ³⁸D. R. Chen and X. L. Jiao, "Solvothermal Synthesis and Characterization of Barium Titanate Powders," *J. Am. Ceram. Soc.*, **83** [10] 2637–9 (2000).
- ³⁹D. Hennings, M. Klee, and R. Waser, "Advanced Dielectrics: Bulk Ceramic and Thin Films," *Adv. Mater.*, **3**, 334–40 (1991).
- ⁴⁰C. J. Howard and H. T. Stokes, "Group-Theoretical Analysis of Octahedral Tilting in Perovskites," *Acta Crystallogr. B*, **54**, 782–9 (1998).
- ⁴¹W. B. White, "The Structure of Particles and the Structure of Crystals: Information from Vibrational Spectroscopy," *J. Ceram. Proc. Res.*, **6** [1] 1–9 (2005). □